Limnol. Oceanogr., 50(5), 2005, 1667–1676

Universal scaling of dissolved oxygen distribution at the sediment–water interface: A power law

Miki Hondzo,[1] *Tom Feyaerts, Richard Donovan,*[2] *and Ben L. O'Connor*
St. Anthony Falls Laboratory, Department of Civil Engineering, University of Minnesota, Mississippi River at 3rd Avenue SE, Minneapolis, Minnesota 55414

Abstract

Dissolved oxygen (DO) distribution at the sediment–water interface of a flow over a smooth bed is investigated for Reynolds numbers >360 and <4,090. These conditions are commonly encountered in streams, wetlands, and lakes. A power-law scaling of DO distribution is derived and compared with experimental data. The scaling analysis is based on DO flux at the sediment–water interface in a turbulent flow. The power-law model with diffusive sublayer thickness (DSLT) as a fitting parameter agrees well with the data over the investigated range of Reynolds numbers. Using the proposed power-law model with a limited number of DO and flow properties away from the sediment–water interface provides the distribution of DO concentrations and corresponding DSLT at a submillimeter resolution. The estimate of DSLT is, on average, 30% lower than the traditional estimate, defined as a thin fluid layer bounded at the lower boundary by a sediment bed and extended upward in the main water column to where a bulk DO concentration intersects with a linear DO gradient at the bed.

The transport processes across the sediment–water interface are of fundamental importance to biological and chemical processes in streams, rivers, and lakes (Boudreau and Jørgensen 2001). In most cases, researchers are concerned about quantifying the distribution and corresponding flux of a particular substance at the sediment–water interface. The dissolved oxygen (DO) concentration in water has been considered one of the most important ecological parameters determining the water quality and associated biological composition of aquatic environments. The sediments, being a repository for decaying biological material with a large organic content, are a major contributor to the DO reduction in the water column.

Significant laboratory and field measurements have been devoted to addressing the DO transport process at the sediment–water interface (e.g., Jørgensen and Des Marais 1990; Mackenthun and Stefan 1998; Røy et al. 2002). Microstructure DO measurements with microsensors (e.g., Jørgensen and Revsbech 1985; Lorke et al. 2003; Røy et al. 2004) have been very instrumental in the advancement of theories and models fundamental to the DO transport at the sediment–water interface. Knowledge of the characteristics of the diffusive sublayer thickness (DSLT) for the DO transport and corresponding DO distribution at the sediment–water interface is crucial in benthic ecology. The difficulty in the characterization of the diffusive sublayer lies in its thinness, usually <5 mm, and the proximity of a solid boundary. Modeling approaches that relate the characterization of the diffusive sublayer to the Reynolds number of the mean flow ($Re_H = UH/\nu$, where U is the mean velocity of flow averaged over the entire boundary layer, H is the boundary layer thickness, and ν is the kinematic viscosity), and the corresponding microscopic length scale at the sediment–water interface (ν/u_*, where u_* is the shear velocity) have been very instrumental. It is well established that for a waterside-controlled DO transport at $Re_H > 3{,}000$, the hydrodynamic conditions in a water column control the thickness of the diffusive sublayer and the corresponding DO flux at the sediment–water interface. At low Reynolds numbers, a functional dependence of DSLT versus small- or large-scale characterization of flow has not been established. The conditions at low Reynolds numbers contain laminar-transition-turbulent flow where the hydrodynamic and mass transport environments may be different from the reported measurements at high Reynolds numbers. Low water velocities ($Re_H < 3{,}000$) that promote the settling of fine sediment particles and associated organic materials with high DO utilization rates are frequently encountered in pools of streams, rivers, flood plains, wetlands, and lakes, and they therefore deserve more research attention.

Even under laboratory conditions, the determination of the vertical distribution of DO and associated DSLT at the sediment–water interface is an experimental challenge. It requires the use of specialized equipment, including fragile DO microsensors, analog current amplifiers, and the detection of the sediment–water interface. Motivated by the usefulness of the universal log-law for momentum transport in a turbulent flow, where shear velocity at the sediment–water interface is determined by fitting the universal log-law to a limited number of velocity measurements away from the sediment bed, researchers have attempted to derive an analytical expression for the universal DO vertical distribution with a free-parameter DSLT.

This article analyzes the effect of fluid motion on DO vertical distribution and transport near the sediment–water

[1] Corresponding author (mhondzo@umn.edu).
[2] Present address: James R. Hill, Inc., 1523 94th Lane NE, Blaine, Minnesota 55449.

Acknowledgments

This paper is a publication of the National Center for Earth-surface Dynamics (NCED), which is founded by the National Science Foundation. Experimental work and preparation of this paper were supported by NCED. The authors are grateful to Christopher Ellis, St. Anthony Falls Laboratory, University of Minnesota, for help with the data acquisition and processing. We gratefully acknowledge the helpful criticism of two unknown reviewers.

Table 1. Notation.*

$\underline{C}$	DO concentration (M L^{-3})
$\bar{C}$	Time-averaged DO concentration (M L^{-3})
C_B	Depth-averaged DO concentration (M L^{-3})
C_S	DO concentration at the sediment–water interface (M L^{-3})
C'	Integration variable (M L^{-3})
C^+	$[(C_S - C)u_*]/J$
D	Molecular diffusion coefficient of DO (L^2 T^{-1})
D_t	Turbulent diffusion coefficient of DO (L^2 T^{-1})
E_t	Turbulent diffusion coefficient of momentum (L^2 T^{-1})
H	Boundary layer thickness (half-distance between the sediments and upper plate) (L)
J	DO flux per unit area (M $L^{-2}T^{-1}$)
k	D/δ_C Local mass transfer velocity (L T^{-1})
Re_H	UH/ν Reynolds number
Sc	ν/D Schmidt number
Sc_t	E_t/D_t Turbulent Schmidt number
Sh	kH/D Sherwood number
$\bar{u}$	Time-averaged velocity (L T^{-1})
U	Mean velocity of flow averaged over the entire boundary layer (L T^{-1})
u_*	Shear or friction velocity (L T^{-1})
X	Downstream distance in flow (L)
Y	Vertical distance from sediment (L)
Z	Lateral distance from the centerline of channel (L)
y^+	yu_*/ν
y'	Integration variable (L)
δ_{DSL}	Diffusive sublayer thickness DSLT (L)
δ_{CB}	Estimated diffusive sublayer thickness from the DO concentration profile (L). The vertical distance from the sediment bed to the point in the water column where the depth-averaged DO concentration, C_B, intersects with the linear gradient of DO concentration at the sediment–water interface.
δ_{CS}	Estimated diffusive sublayer thickness from the concentration similarity group (L). Inverse of the slope of dimensionless similarity group at the sediment–water interface (Eq. 9).
δ_{CP}	Estimated diffusive sublayer thickness from the universal power law (L). The vertical distance from the sediments to the point in the water column where the molecular diffusion is the dominant transport process over the turbulent diffusion.
δ_v	Viscous sublayer thickness (L)
δ^+_{CP}	δ_{CP} u_*/ν
κ	von Kármán's constant (0.41)
ν	Kinematic viscosity of fluid (L^2 T^{-1})

* M, mass; L, length; T, time.

interface in a laboratory flume at low Reynolds numbers. Microstructure DO measurements will be augmented with small-scale flow measurements at low Reynolds numbers under laboratory conditions. The traditional definition of DSLT (Boudreau and Jørgensen 2001) as well as alternative formulations will be investigated. The dimensional parameters relating cross-sectional averaged parameters to DSLT will be used in the analysis of data. With a reliance on the established flux laws of mass and momentum transports at the solid-water interface, a power-law scaling of the vertical distribution of DO concentrations will be derived and compared by measurements. The power law provides an estimate of DSLT, while the molecular diffusion of DO is the dominant transport process. A list of notations is provided in Table 1.

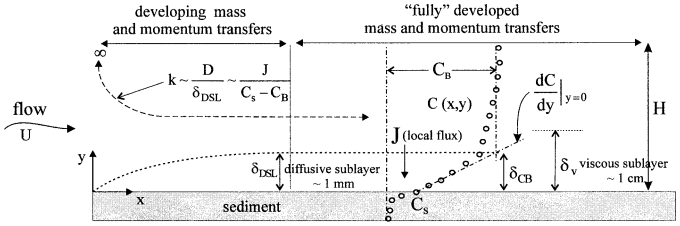

Fig. 1. Conceptual sketch for developing and developed near-bed concentration and velocity distributions. U is the mean velocity of flow averaged over the entire boundary layer, H is the boundary layer thickness, k is the mass transfer velocity, D is the molecular diffusion coefficient, δ_{DSL} is the DO diffusive sublayer thickness, C_B is the bulk concentration, C_s is the concentration at the sediment–water interface, δ_{CB} is the traditional definition of diffusive sublayer thickness, and δ_v is the momentum diffusive sublayer.

Theoretical background

The dimensionless analysis of cross-sectional averaged flow characteristics and DO concentration above the sediment–water interface in a moving fluid, where a reaction at the sediment surface is causing a reduction in DO concentration in the fluid above, suggests that the DO mass transfer is governed by the following parameters (e.g., Steinberger and Hondzo 1999):

$$\mathrm{Sh} = f(\mathrm{Re}_H, Sc) = \frac{\frac{D}{\delta_{DSL}}H}{D} = f\left(\frac{UH}{\nu}, \frac{\nu}{D}\right) \qquad (1)$$

where Sh is the Sherwood number, $f(\,)$ is the unknown function, Sc is the Schmidt number, D is the molecular diffusion coefficient for DO, and δ_{DSL} is the DSLT. For a given Schmidt number, the DSLT is a function of the Reynolds number. While the dimensionless analysis provides a systematic summary of parameters that govern the process, it does not determine the form of the function $f(\,)$. To determine the nature of the function $f(\,)$ without empiricism, it is necessary to consider governing laws of mass and momentum transfers at the sediment–water interface.

Consider a flow with a high DO concentration moving over a smooth bed in a laboratory flume with low DO concentrations in the bed (Fig. 1). As the fluid proceeds along the channel, concentration and velocity boundary layers form adjacent to the bed. These boundary layers grow in a streamwise direction until no further changes occur in the time-averaged DO concentrations and velocity characteristics. The flow becomes fully developed, meaning the concentration and velocity profiles are unchanging in the streamwise direction. The velocity sublayer close to the bed is called the viscous sublayer, scaled by $\delta_v \sim a(\nu/u_*)$, where "a" is a constant. The DSLT is scaled by $\delta_{DSL} \sim \delta\nu(D/\nu)^{1/3}$ (Probstein 1989). Since the molecular diffusion coefficient for the DO is 1,000 times smaller than the ν, it is obvious the DSLT should be smaller than the viscous sublayer. The DSLT is "submerged" in the viscous sublayer.

A local DO flux at the sediment–water interface at specified location x along the channel is characterized by the first Fick's law.

$$J = -D\left.\frac{dC}{dy}\right|_{y=0} \tag{2}$$

where C is the DO concentration, y is the vertical distance from the sediment bed upward, $(dC/dy)|_{y=0}$ is the local concentration gradient that is located at distance (x), and J is the local DO flux per unit area. An alternative formulation for the local DO flux at the sediment–water interface can be defined as follows (e.g., Jørgensen and Revsbech 1985):

$$J = -k(C_B - C_S) = -\frac{D}{\delta_{\mathrm{DSL}}}(C_B - C_S) \tag{3}$$

where $k = D/\delta_{\mathrm{DSL}}$ is the local mass transfer coefficient, C_S is the DO concentration at the sediment–water interface,

$$C_B = \frac{\int_0^H u(C - C_S)\, dy}{\int_0^H u\, dy} + C_S$$

is the depth-averaged DO concentration, and u is the velocity in the downstream (x) direction. Traditionally, DSLT, δ_{DSL}, is defined as the vertical distance from a sediment bed to the upward location in the main water column where the depth-averaged DO concentration intersects with the linear DO gradient at the sediment–water interface $(dC/dy)|_{y=0}$ (Jørgensen and Revsbech 1985). Subsequently, this paper will refer to the traditional estimate of DSLT by the symbol δ_{CB}. The thickness is determined by a graphical procedure (Fig. 1). The commonly used definition of DO flux by Eq. 3 implies that the DSLT molecular diffusion is the dominant transport process.

Using a similarity argument, Steinberger and Hondzo (1999) proposed that in a developed flow, the concentration similarity group $f = (C - C_S)/(C_B - C_S)$ should not change in the streamwise flow direction.

$$\frac{df}{dx} = \frac{d}{dx}\left(\frac{C - C_S}{C_B - C_S}\right) = 0 \tag{4}$$

Integrating Eq. 4,

$$\left(\frac{C - C_S}{C_B - C_S}\right) = f(y) \tag{5}$$

Therefore, since

$$C = C_S + (C_B - C_S)f(y) \tag{6}$$

the local DO concentration gradient is

$$\frac{dC}{dy} = (C_B - C_S)\frac{df}{dy} \tag{7}$$

Using Eq. 2, the local DO flux at the sediment–water interface is

$$J = -D\left.\frac{dC}{dy}\right|_{y=0} = -D(C_B - C_S)\left.\frac{df}{dy}\right|_{y=0} \tag{8}$$

Equating Eqs. 3 and 8, a reformulation of the estimate of DSLT follows:

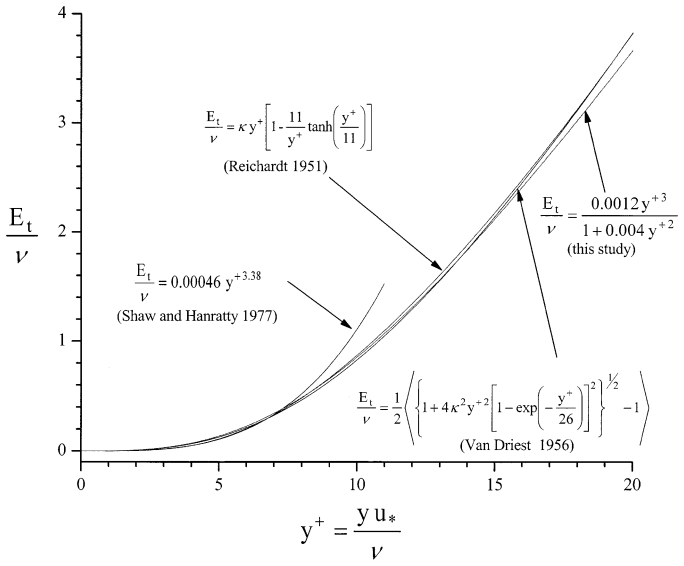

Fig. 2. Turbulent diffusion coefficient variability versus dimensionless distance from the sediments upward in the water column. κ is the von Kármán's constant (0.41), and y^+ is the dimensionless "wall" coordinate $y^+ = yu_*/\nu$.

$$\delta_{\mathrm{CS}} = \frac{1}{(df/dy)|_{y=0}} \tag{9}$$

where $(df/dy)|_{y=0}$ is the local gradient of the concentration similarity group, evaluated at the sediment–water interface, and δ_{CS} is the estimate of DSLT determined by the slope of similarity group at the sediment–water interface. Since the concentration similarity group should not change in the streamwise flow direction for given conditions in a developed flow, the DSLT given by Eq. 9 should be constant. The invariance of the DO concentration similarity group and constant DSLT are characteristics of the developed mass transfer, theoretically postulated by Hondzo and Steinberger (2002). Conceptually, there is no difference between δ_{CB} and δ_{CS}. However, δ_{CS} is determined by a similarity group, supposedly invariant for given flow conditions in a developed flow, while δ_{CB} is determined by DO data, not necessarily invariant for given flow conditions in the developed flow.

In a turbulent flow, the total diffusive flux of DO in the y direction is given by

$$J = -(D + D_t)\frac{d\bar{C}}{dy} \tag{10}$$

where D_t is the eddy diffusion coefficient or turbulent diffusion coefficient for DO transfer, and $\bar{C}$ is the time-averaged DO concentration. The eddy diffusivity for momentum and the eddy diffusivity for mass are related through the turbulent Schmidt number $\mathrm{Sc}_t = E_t/D_t$, where E_t is the turbulent diffusion coefficient for momentum transfer. Several different algebraic turbulence models for E_t have been proposed (Reichardt 1951; Van Driest 1956; Shaw and Hanratty 1977). All models are empirical, depict similar vertical distance dependence of E_t, and display a common rapid decrease in E_t as the solid surface is approached (Fig. 2).

Let us now restrict the consideration to the region near

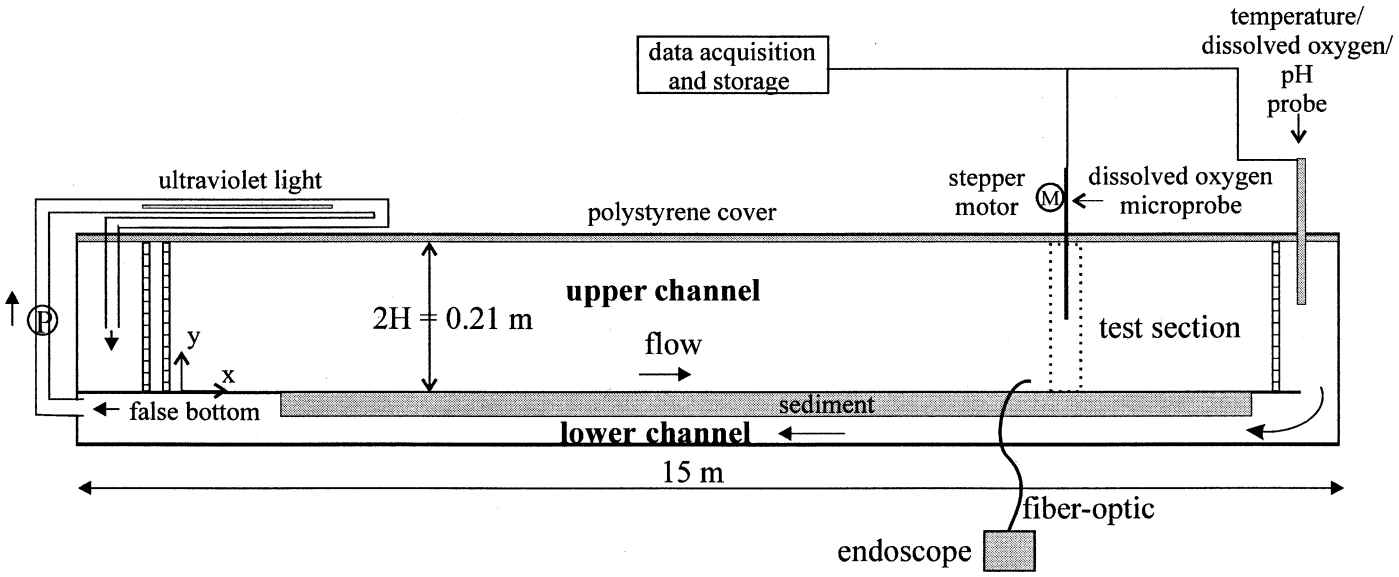

Fig. 3. Experimental setup at the St. Anthony Falls Laboratory.

the sediment bed and integrate Eq. 10 from $y = 0$ upward in the main water column. Thus, we obtain

$$\int_{C_s}^{C'} d\bar{C} = -\int_0^{y'} \frac{J}{D + D_t}\, dy \tag{11}$$

Substituting the definition of wall distance, $y^+ = yu_*/\nu$, and nondimensional concentration $C^+ = [(\bar{C} - \bar{C}_S)u_*]/J$ in Eq. 11, we obtain

$$C^+ = \frac{(\bar{C} - \bar{C}_S)u_*}{J} = -\int_0^{y^{+\prime}} \frac{dy^+}{\frac{D}{\nu} + \frac{D_t}{\nu}}$$

$$= -\int_0^{y^{+\prime}} \frac{dy^+}{\frac{1}{\mathrm{Sc}} + \frac{E_t}{\mathrm{Sc}_t \nu}} \tag{12}$$

Considering a concept of a two-layer model where the layers are in communication (e.g., Røy et al. 2004) with a diffusive sublayer at the sediment–water interface and turbulent flow in the remaining water column, we can decompose the integral on the right-hand side of Eq. 12:

$$-C^+ = \int_0^{\delta_{\mathrm{CP}}^+} \frac{dy^+}{\frac{1}{S_c} + \frac{E_t}{S_{\mathrm{ct}}\nu}} + \int_{\delta_{\mathrm{CP}}^+}^{y^{+\prime}} \frac{dy^+}{\frac{1}{S_c} + \frac{E_t}{S_{\mathrm{ct}}\nu}} \tag{13}$$

where $\delta_{\mathrm{CP}}^+ = (\delta_{\mathrm{CP}}u_*)/\nu$ is the dimensionless estimate of DSLT, and δ_{CP} is the dimensional estimate of DSLT. We assume that in the diffusive sublayer δ_{CP} region, 1/Sc dominates over E_t/ν and, therefore, we will neglect E_t/ν in the first integral on the right-hand side of Eq. 13. Outside δ_{CP}, E_t/ν dominates over 1/Sc and, thus, we will neglect 1/Sc in the second integral on the right-hand side. This approximation explicitly implies that the molecular diffusion of DO is the dominant transport process over δ_{CP} and provides the third estimate of DSLT. Implying the simplifications, Eq. 13 reads

$$-C^+ = \int_0^{\delta_{\mathrm{CP}}^+} \frac{dy^+}{\frac{1}{\mathrm{Sc}}} + \int_{\delta_{\mathrm{CP}}^+}^{y^{+\prime}} \frac{dy^+}{\frac{E_t}{\mathrm{Sc}_t\nu}} \tag{14}$$

To provide an analytical expression for C^+, we have to integrate Eq. 14. This step requires an expression for E_t/ν. Unfortunately, the expressions of E_t/ν available in the literature (Fig. 2) cannot be analytically integrated in Eq. 14. Comparing the existing equations with expressions that can be integrated (Fig. 2), we propose the following:

$$\frac{E_t}{\nu} = \frac{0.0012y^{+3}}{1 + 0.004y^{+2}} \tag{15}$$

Substituting Eq. 15 in Eq. 14, integrating, and simplifying, we obtained

$$C^+ = \begin{cases} y^+\mathrm{Sc} & \text{for } y^+ < \delta_{\mathrm{CP}}^+ \\ \delta_{\mathrm{CP}}^+\mathrm{Sc} + \mathrm{A}\mathrm{Sc}_t \ln\left(\dfrac{y^+}{\delta_{\mathrm{CP}}^+}\right) + \mathrm{B}\mathrm{Sc}_t\left(\dfrac{1}{\delta_{\mathrm{CP}}^{+2}} - \dfrac{1}{y^{+2}}\right) & \text{for } y^+ \geq \delta_{\mathrm{CP}}^+ \end{cases} \tag{16}$$

where A = 3.4 and B = 417 are the constants of integration. Equation 16 provides a power-law scaling for the DO distribution. The universality of the proposed expression and possible simplifications at different Reynolds numbers will be elaborated on using our microstructure DO measurements.

Experimental setup and procedure

Flow setup—The general setup of the equipment is visualized in Fig. 3. Measurements were performed in a 15.0-m-long, 0.6-m-wide, and 0.4-m-deep flume with glass walls

at the St. Anthony Falls Laboratory, University of Minnesota. Fluid flow in the channel was bounded by bottom sediments and a freely floating polystyrene cover. The water depth in the channel was constant in all experiments and equal to $2H = 21$ cm. The flume has to be long enough to ensure a fully developed mass and momentum boundary layers at the sediment–water interface. Previous studies in the same flume on the bulk reduction of DO in a water column demonstrated the existence of a fully developed momentum boundary layer, independent of cross-channel positions over $z/H \leq 2.3$ from the centerline of the channel (Mackenthun and Stefan 1993). The flume was divided in an upper channel, in which the measurements were taken, and a lower channel, which guided the return flow. The sediments were 2.5 cm thick and were contained in a false bottom along an 11-m reach of the upper channel. They consisted of sawdust mixed with agar, which is a gelatinous substance extracted from sea kelp. The flume was consistently filled to the same height to ensure that equal volumes of water were tested in each experiment. The flow and, consequently, the velocity through the channel were controlled by a 5-Hp centrifugal pump. The range of flow rates possible with this equipment was 0.4–4.0 L s^{-1}. To be able to set the flow to the appropriate value, a calibrated orifice located downstream of the pump was used. The flow velocities were measured by an acoustic-Doppler velocimeter (ADV), taken in the upper channel.

Several precautions were taken to reduce the impact of other oxygen sources and sinks in the channel. On top of the water in the upper channel, the polystyrene cover was placed to reduce reaeration from the atmosphere. To reduce oxygen consumption by microorganisms in the water itself, a high-intensity ultraviolet disinfection lamp with an output of 30 μW cm^{-2} was mounted in the recirculation path of the pump to limit microbial growth. The specific rate of oxygen uptake was assumed to be constant during the period of the measurements. Having prescribed a mixture for sediments and minimized DO sources and sinks in the water above sediments, the experiments were reproducible with identical initial and boundary conditions where the change in mass flux could be attributed to a change in flow.

Measuring devices—The measurements include the use of a velocity probe (ADV), a water quality probe, and a microprobe for obtaining detailed DO profiles near the sediment–water interface. The placement of these different devices is schematically shown in Fig. 3. The positioning of the ADV probe was done with a micrometer in combination with a screw assembly. An average of 2,000 samples measured at 20-Hz frequency were acquired per measuring point. The velocities were measured in three dimensions, and the data were used to calculate streamwise depth-averaged velocity and shear stress velocity. A Hydrolab Datasonde 3 multiparameter probe was used to measure bulk parameters in the water column, including water temperature, pH, and DO concentration. Samples were taken at 10-min intervals. The online display of time series of measured bulk parameters provided an inspection of the hypothesis of constant environmental conditions in the channel during the measurements.

The oxygen concentration profiles were recorded with Unisense OX-10 and OX-20 microprobes, which are miniaturized Clark-type oxygen sensors with an internal reference and a guard cathode. The sensor was connected to a high-sensitivity Unisense PA2000 ammeter, with a short-signal 90% response time of 1.0 s. The OX-10 and OX-20 microprobes used have an outer tip diameter of 10 and 20 μm, respectively, which makes them very fragile. This small diameter allows DO measurements for very small traverse distances, which is necessary to collect data in the boundary layer. A drawback of the probes is the fragility of their tip, which puts restrictions on the roughness of the sediment used. Readings were taken in pA, and the DO values were calculated using the calibration values and applying a temperature and pressure correction. The positioning of the DO microprobe was done by using a computer-controlled stepper motor with a 0.001-mm resolution. Previous research (Oldham 1994; Steinberger and Hondzo 1999) concluded that the effect of velocity on the reading was negligible but that the microprobe drifts with time, so a recalibration of the probe prior to and at the end of every experiment is required.

Experimental procedure—The water in the flume was changed prior to every experimental run. The tip of the DO microprobe was carefully positioned at the sediment–water interface by visual judgment. The visualization was performed by using an endoscope that has a 65-cm-long flexible shaft and an internal light source that illuminates the image through fiber-optic strands, each having a diameter of 3 μm. The judgment of the position of the interface is a critical step in the experimental procedure, because it determines the origin of the DSLT. Once the interface was determined, the microprobe was raised 10 cm with the computer-controlled stepper motor to the position where the first sample was taken. The channel was sealed with the polystyrene cover, except for a small opening for the microprobe. The flow was set to the desired flow rate, and then the system was allowed to stabilize for at least 4 h to ensure uniform flow, temperature, and DO throughout the channel. Bulk DO readings and temperature data with online display were recorded by the Hydrolab probe during a 4-h period. After the system was stabilized, the microprofile was taken by gradually lowering the microprobe in the channel. At each sampling location, 250 samples were taken, and the readings of the picoammeter were channeled to a computer, where time-averaged data were recorded.

The disturbance of the flow by the cylindrical-measuring DO microelectrode and the corresponding possible effect on the DSLT were considered. The problem pertains to the flow disturbance caused by the microelectrode stem and its tip. The placement of the microelectrode in the experimental setup with the associated flow conditions can have a significant effect on the DSLT (Glud et al. 1994; Lorenzen et al. 1995; Røy et al. 2004). The microelectrode measurements from above, from the water column downward toward the sediments, can cause the compression of the DSLT by 25–45% (Glud et al. 1994; Lorenzen et al. 1995). The potential effect of compression on the DSLT can be more amplified, especially in experimental reactors without developed flow conditions. We have quantified the disturbance of the flow by

Table 2. Summary of measured and estimated experimental parameters.

Exp.	$2H$ (cm)	U (cm s^{-1})	$\mathrm{Re_H}=\frac{UH}{\nu}$ (−)	u_* (cm s^{-1})	C_B (mg L^{-1})	C_s (mg L^{-1})	D (cm^2 s^{-1})	Sc (−)	$y=\delta_{CS}$ (mm)	$y=\delta_{CB}$ (mm)	$y=\delta_{CP}$ (mm)	$\frac{1}{\mathrm{Sc}}=\frac{D}{\nu}$ (−)	$\frac{E_t}{\nu}$ (−)	$\frac{E_t^*}{\nu}$ (−)	$\frac{E_t/\nu - D/\nu}{D/\nu}$ (%)
A-1	21	0.34	363	0.042	8.40	2.98	1.80×10^{-5}	544	3.54	3.88	2.80	0.0018	0.0055	0.0052	206
A-2	21	0.56	677	0.050	8.83	4.28	2.08×10^{-5}	419	3.39	3.69	2.43	0.0024	0.0112	0.0106	367
A-3	21	0.86	833	0.069	5.33	0.42	1.61×10^{-5}	672	2.53	2.80	1.88	0.0015	0.0067	0.0064	347
A-4	21	1.39	1,731	0.097	4.12	0.21	2.16×10^{-5}	391	1.69	1.88	1.31	0.0026	0.0118	0.0112	354
A-5	21	1.72	1,766	0.112	8.16	4.93	1.72×10^{-5}	596	1.52	1.63	0.96	0.0017	0.0068	0.0063	300
A-6	21	2.36	2,983	0.146	4.68	2.36	2.21×10^{-5}	377	1.20	1.35	0.68	0.0027	0.0155	0.0148	474
A-7	21	2.53	2,841	0.156	7.33	5.47	1.91×10^{-5}	489	0.99	0.95	0.72	0.0020	0.0047	0.0045	135
A-8	21	3.04	2,454	0.178	11.69	8.73	1.30×10^{-5}	996	1.05	0.97	0.80	0.0010	0.0028	0.0027	180
A-9	21	3.29	4,092	0.191	8.10	1.25	2.17×10^{-5}	389	0.78	0.89	0.62	0.0026	0.0096	0.0091	269

* $E_t/\nu = \kappa y^+[1 - (11/y^+)\tanh(y^+/11)]$ (Reichardt 1951).

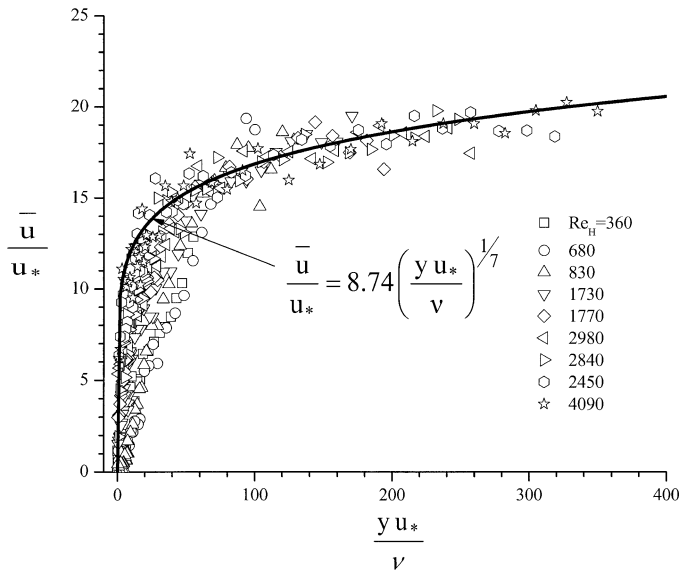

Fig. 4. Time-averaged velocity distributions versus dimensionless distance at x = 10.0 m at the channel centerline.

the microelectrode stem in our laboratory flume with the unidirectional parallel shear flow. Dimensional analysis shows that a dimensionless frequency, the Strouhal number, depends on the Reynolds number of the flow. The maximum Reynolds number with the velocity scale at the top of DSLT and the length scale equal to the diameter (d) of the microelectrode, completely submerged in the DSLT, is about Re = $(ud)/\nu \approx 6$. The flow regime corresponds to the regime of the unseparated flow behind the cylinder (Lienhard 1987). Therefore, the disturbance of the flow by the microelectrode stem was considered minimal.

Results

Flow measurements—Experiments were conducted at nine different velocities, corresponding to Reynolds numbers ranging from 360 to 4,090 (Table 2). Time-averaged velocity distributions were fitted to the log-law velocity distribution, $\bar{u}/u_* = (1/\kappa)\ln(y) + \text{constant}$, close to the sediments, or the inner region/wall region (Schlichting 1979), and provided the estimates of shear stress velocity at the bed (Table 2). The one-seventh power velocity distribution is well established for turbulent flows over smooth boundaries and agrees well with the measured velocities, especially in the region $(yu_*)/\nu > 50$, where the power law should be in agreement with the universal logarithmic velocity distribution (Fig. 4).

DO microprofiles—An example of DO microprofiles at two distant Reynolds numbers, measured at 9.0, 10.0, and 11.0 m of the upstream edge of the flume with sediments, is provided in Fig. 5. The similarity group $\bar{f} = [(C - C_S)/(C_B - C_S)]$ versus normalized depth, y/H, displays identical profiles at different locations along the flume. This plot demonstrates both profiles were measured in a developed flow where individual concentrations may change along the channel, as $C(y)$ obviously does. However, the similarity group, $\bar{f}$, should not change at different locations.

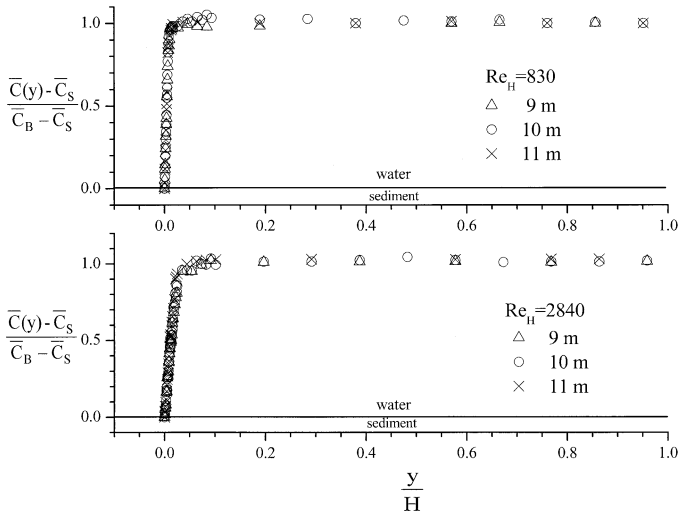

Fig. 5. Dimensionless similarity group concentrations of dissolved oxygen at $x = 9.0$ m, $x = 10$ m (test section), and $x = 11$ m at the channel centerline.

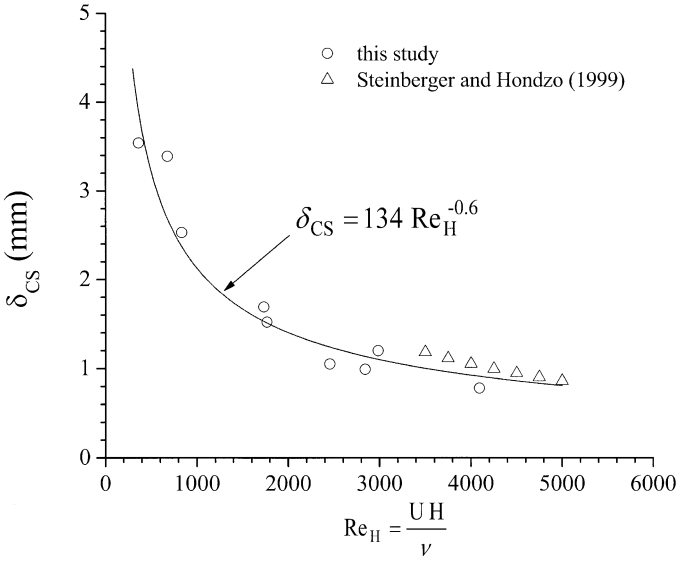

Fig. 7. Diffusive sublayer thickness (δ_{CS}) dependence on flow conditions (Re_H).

Nine different DO microprofiles were obtained at different flow velocities (Fig. 6). All microprofiles were taken at a location 10.0 m of the upstream edge of the sediments in the centerline of the channel. In the main water column, the almost constant mean DO concentration was reduced toward the sediments because of the downward DO flux, i.e., from the water toward the sediment bed. The DSLT, δ_{CS}, based on measurements and Eq. 9, decreased with larger Reynolds numbers, indicating larger DO flux with Reynolds numbers. The traditional estimates of DSLT, δ_{CB}, and the estimates of δ_{CS} by the similarity provided similar results (Table 2). On average, δ_{CB} was 6% larger than the estimate of δ_{CS}. While the determination of the bulk DO concentration is a relatively straightforward procedure, the determination of the linear DO gradient at the sediment–water interface is less straightforward and involves subjective judgment (e.g., Fig. 6, profiles at $Re_H = 680$ and $Re_H = 1{,}730$).

A functional dependence between δ_{CS} and the Reynolds number is provided in Fig. 7. A power-law behavior is evident in good agreement with the previous research at higher Reynolds numbers (Steinberger and Hondzo 1999). The δ_{CS} is also plotted as a function of the wall variables and Schmidt number (Fig. 8). As at higher Reynolds numbers (Steinberger and Hondzo 1999), DSLT scales very well with the wall variables.

Universal power-law scaling—To investigate whether the theoretical model for the power-law scaling (Eq. 16) results in a universal law, the dimensionless concentration $C^+ =$

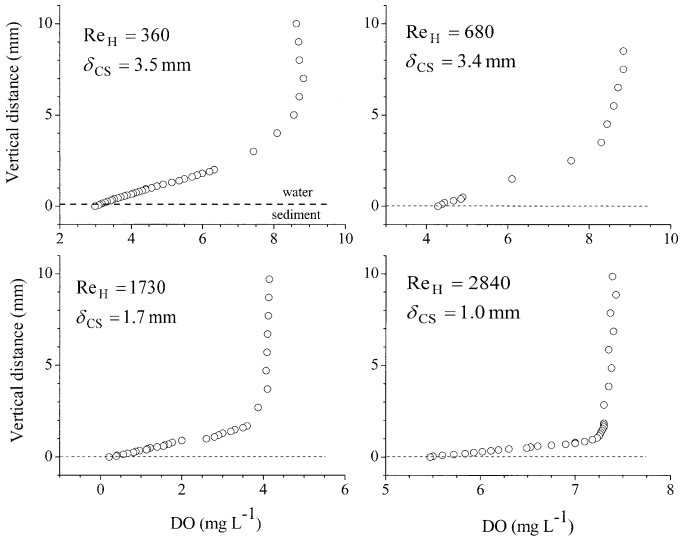

Fig. 6. Dissolved oxygen concentration profiles in the near-sediment region at different fluid flow conditions.

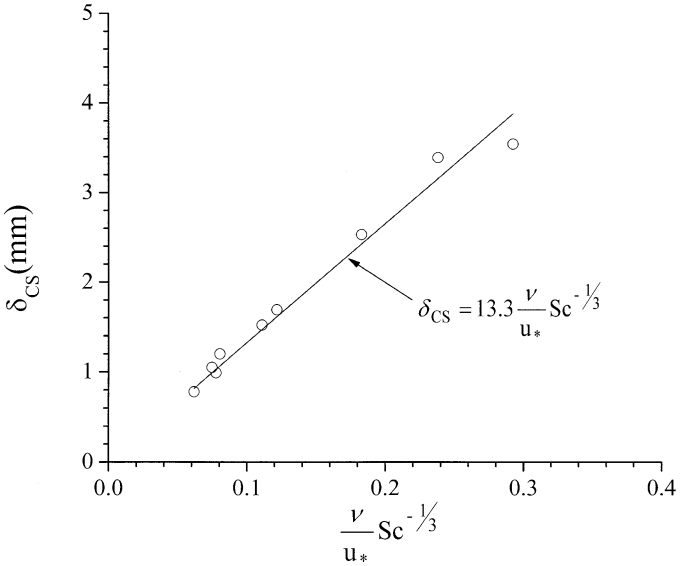

Fig. 8. Diffusive sublayer thickness (δ_{CS}) dependence on viscous length scale (ν/u_*) and Schmidt number (Sc).

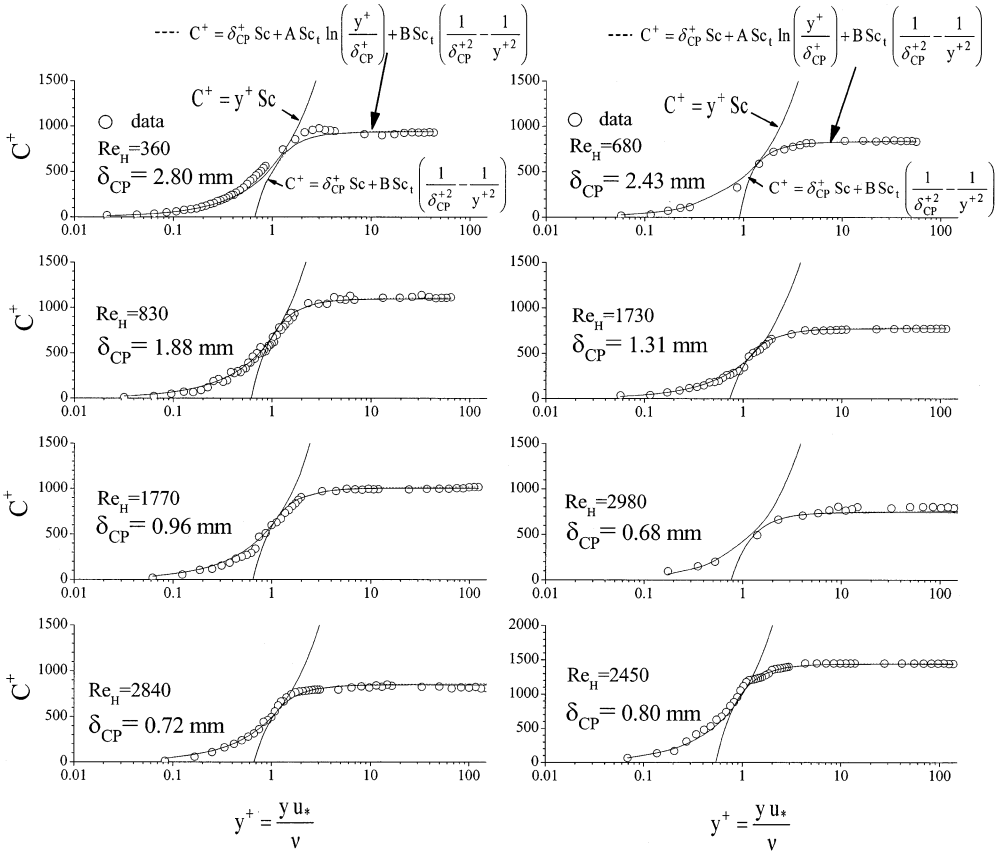

Fig. 9. Dimensionless dissolved oxygen concentration profiles versus dimensionless distance from the sediments upward in the water column at different flow conditions.

$[(\bar{C}_s - \bar{C})u_*]/J$ was plotted against the logarithm of the dimensionless depth $y^+ = (yu_*)/\nu$ (Fig. 9). Very close to the sediment, the dimensionless concentration scale is $C^+ \sim (y^+)S_c$ or the solution of first integral in Eq. 14. Away from the sediment bed, $y^+ \geq \delta_{CP}^+$, the distribution of the concentration scale as the proposed power law in Eq. 16. Initially, two fitting parameters, δ_{CP}^+ and Sc_t, were used to fit the proposed power law to the data. The constants A = 3.4 and B = 417 were unchanged in all profiles. The turbulent Schmidt number was equal to 1 in all experiments except for Sc_t = 0.9 at Re = 360. Therefore, δ_{CP}^+ was the only fitting parameter. Very good agreement between the data and proposed model is evident. The estimated DSLT, $\delta_{CP} = (\delta_{CP}^+\nu)/u_*$, displayed similar behavior as depicted in Fig. 7, where the higher Reynolds number caused lower DSLT and, therefore, larger DO flux. The comparison of δ_{CP} and the traditional estimate of DSLT by δ_{CB} indicated that, on average, δ_{CB} was 30% larger than the δ_{CP} (Table 2). An inspection of D/ν = 1/Sc and E_t/ν (proposed in this study) or E_t/ν (proposed by Reichardt 1951) at the top of δ_{CB} indicates $E_t/\nu \gg D/\nu$ (Table 2). The depth at which the two relative diffusivities were comparable, $E_t/\nu \approx D/\nu$, was, on average, 30% smaller than the traditional DSLT δ_{CB}. Although E_t/ν was, on average, 300% larger than D/ν at the top of δ_{CB}, the fact that E_t/ν tends to zero rapidly close to the solid boundary makes the two diffusivities comparable at a height 30% smaller than δ_{CB}. The DSLT δ_{CP} was submerged in δ_{CB}.

The dimensionless sublayer thickness δ_{CP}^+ was on the order of 1 over the range of investigated Reynolds numbers (Fig. 9). An inspection of different terms in Eq. 16 revealed that the magnitude of A $\ln(y^+/\delta_{CP}^+)$ was insignificant in comparison to the rest of the terms in Eq. 16. Neglecting term A $\ln(y^+/\delta_{CP}^+)$ in Eq. 16, a simplified power law is obtained where

$$C^+ = \begin{cases} y^+ Sc & \text{for } y^+ < \delta_{CP}^+ \\ \delta_{CP}^+ Sc + BSc_t\left(\dfrac{1}{\delta_{CP}^{+2}} - \dfrac{1}{y^{+2}}\right) & \text{for } y^+ \geq \delta_{CP}^+ \end{cases} \quad (17)$$

The results were compared in Fig. 9. The full analytical version of the power law (Eq. 16) is depicted by a dashed line, and the simplified version (Eq. 17) is displayed by a solid line. The differences in results are negligible, so it is difficult to distinguish between the dashed and solid lines. Independently, both laws provided identical estimates of δ_{CP}^+ and the corresponding DSLT δ_{CP}.

A functional relationship between the estimated δ_{CP} and Reynolds number is provided in Fig. 10. For comparison, the estimates of δ_{CS} are provided on the same graph. The individual estimates of δ_{CP} were, on average, 30% smaller than the δ_{CS}. In either case, a functional relationship of the estimated DSLT versus Reynolds number is proposed by $\delta_{CP} \approx \delta_{CS} \approx$ con $Re_H^{-0.6}$.

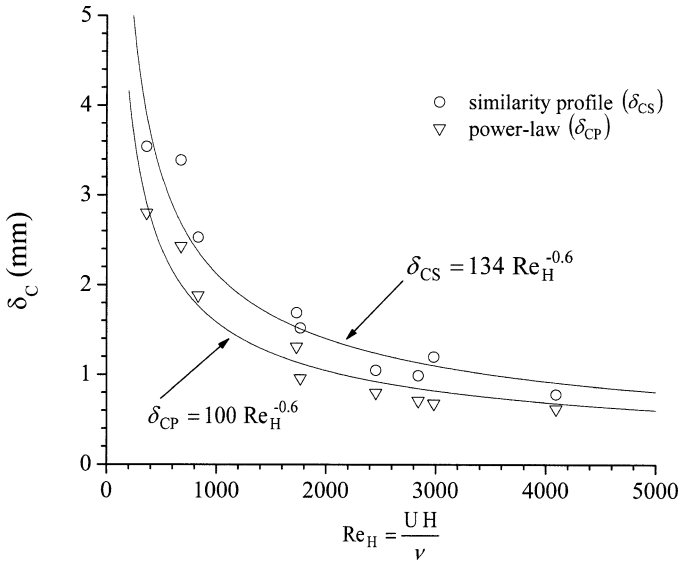

Fig. 10. Comparison between the diffusive sublayer thickness (δ_{CS}) estimated by using the dissolved oxygen concentration similarity group (Eq. 9) and diffusive sublayer thickness (δ_{CP}) estimated by using the proposed power law (Eq. 17) at different flow conditions, which are characterized by Reynolds numbers.

Discussion

We have investigated the mass flux at the sediment–water interface of a flow over a smooth bed for Reynolds numbers <4,090. These flow conditions are frequently observed in streams, lakes, and wetlands. Experimental work was conducted to measure detailed microprofiles of the DO concentration and velocity profiles in a laboratory flume. The invariance of the concentration similarity group and the constant DSLT are important characteristics of the time-averaged developed flow and are therefore theoretically and experimentally demonstrated in this study.

Three different methods were used to determine the DSLT at the sediment–water interface. The methods included (1) δ_{CB}, the traditional estimate, based on bulk DO concentration and DO gradient through a thin region at the sediment–water interface; (2) δ_{CS}, the estimate elaborated on in this study, based on the concentration similarity group; and (3) δ_{CP}, the estimate based on the derived scaling power law of DO distribution. The estimates of δ_{CB} were similar to the estimates of δ_{CS}. The estimates of δ_{CS} were invariant for the location along the channel in the developed flow and did not require a graphical procedure in the estimation process. Neither method warranted that the molecular diffusion of DO was the dominant transport mechanism within the DSLT. This implies the inadequacy of the commonly used expression for a local DO flux as provided by Eq. 3, where the molecular diffusion coefficient is used as the transport mechanism over the DSLT. The depth at which normalized turbulent diffusion and molecular diffusion of DO were comparable in magnitude, $E_t/\nu \approx D/\nu$, was, on average, 30% smaller than the estimates of δ_{CB} and δ_{CS}. The estimates of δ_{CP} by the proposed universal power law explicitly imply that the molecular diffusion coefficient dominates over the turbulent diffusion within DSLT. The δ_{CP} is estimated by fitting the proposed power law for universal scaling of DO distribution (Eq. 17) to time-averaged DO data. On average, δ_{CP} was 30% smaller than δ_{CB} and δ_{CS}. That the diffusive sublayer, in the proximity above sediments, is not restricted to molecular diffusion only, was suggested by Güss (1998).

A proposed power law for the universal scaling of DO distribution (Eq. 17) with only one fitting parameter, DSLT, has very good agreement with the laboratory measurements. The model considers a formulation for a turbulent diffusion coefficient propagating through the traditionally defined diffusive sublayer, δ_{CB}, next to the sediment–water interface (Boudreau and Jørgensen 2001). This confirms recent findings that a diffusive sublayer, as traditionally defined, is not a quiescent region next to the sediments. Rather, it is a region where DO concentrations and corresponding flux are in periodic communication with the mean flow (Røy et al. 2004). Through the proposed turbulent diffusion coefficient in our model, the upper boundary of DSLT was in communication with the mean flow characteristics.

Measurements of DO concentrations and the delineation of the corresponding DO profile in the proximity of sediments vertically over a couple of millimeters is a difficult task. The detection of the sediment–water interface is another complication that requires specialized equipment. The proposed power law for the universal scaling of the DO distribution is aimed to overcome these difficulties. Having information on flow conditions as characterized by u_* and a limited number of bulk DO concentrations away from the sediment–water interface, the proposed power law can be fitted to the data providing the distribution of DO concentrations and an estimate of DSLT at microscopic scales. These formulations provide a foundation at subgrid scales for numerical simulation models, where the prediction variables at scales smaller than the grid size are parameterized by functional relationships (e.g., Piomelli 1999).

References

BOUDREAU, P. B., AND B. B. JØRGENSEN. 2001. The benthic boundary layer: Transport processes and biogeochemistry. Oxford Univ. Press.

GLUD, R. N., J. K. GUNDERSEN, N. P. REVSBECH, AND B. JØRGENSEN. 1994. Effects on the benthic boundary layer imposed by microelectrodes. Limnol. Oceanogr. **39:** 462–467.

GÜSS, S. 1998. Oxygen uptake at the sediment–water interface simultaneously measured using a flux chamber method and microelectrodes: Must a diffusive boundary layer exist? Estuarine Coastal Shelf Sci. **46:** 143–156.

HONDZO, M., AND N. STEINBERGER. 2002. A semi-analytical model for dissolved oxygen mass transfer coefficient at the sediment–water interface. Hydrobiologia **479:** 63–68.

JØRGENSEN, B. B., AND D. J. DES MARAIS. 1990. The diffusive boundary layer of sediments: Oxygen microgradients over a microbial mat. Limnol. Oceanogr. **35:** 1343–1355.

———, AND N. P. REVSBECH. 1985. Diffusive boundary layers and the oxygen uptake of sediments and detritus. Limnol. Oceanogr. **30:** 111–122.

LIENHARD, H. J. 1987. A heat transfer textbook, 2nd ed. Prentice-Hall.

LORENZEN, J., R. N. GLUD, AND N. P. REVSBECH. 1995. Impact of microsensor-caused changes in diffusive boundary layer thick-

ness on O2 profiles and photosynthetic rates in benthic communities of microorganisms. Mar. Ecol. Prog. Ser. **119:** 237–241.

LORKE, A., B. MÜLLER, M. MAERKI, AND A. WÜEST. 2003. Breathing sediments: The control of diffusive transport across the sediment–water interface by periodic boundary-layer turbulence. Limnol. Oceanogr. **48:** 2077–2085.

MACKENTHUN, A. A., AND H. G. STEFAN. 1993. Experimental analysis of sedimentary oxygen demand in lakes: Dependence on near-bottom flow velocities and implications for aerator design. Univ. of Minnesota, St. Anthony Falls Laboratory, Project Report No. 344.

———, AND ———. 1998. Effect of flow velocity on sediment oxygen demand: Laboratory measurements. J. Environ. Eng. **12:** 222–230.

OLDHAM, C. 1994. A fast-response oxygen sensor for use on finite-scale and microstructure CTD profilers. Limnol. Oceanogr. **39:** 1959–1966.

PIOMELLI, U. 1999. Large-eddy simulation: Achievements and challenges. Prog. Aerosp. Sci. **35:** 335–362.

PROBSTEIN, R. 1989. Physicochemical hydrodynamics: An introduction. Butterworths.

REICHARDT, H. 1951. ''Vollständige Darstellung der turbulenten Geschwindigkeitsverteilung in glatten Leitungen.'' Z. a. M.M. **31:** 208–219.

RØY, H., M. HÜTTEL, AND B. B. JØRGENSEN. 2002. The role of small-scale sediment topography for oxygen flux across the diffusive boundary layer. Limnol. Oceanogr. **47:** 837–847.

———, ———, AND ———. 2004. Transmission of oxygen concentration fluctuations through the diffusive boundary layer overlying aquatic sediments. Limnol. Oceanogr. **49:** 686–692.

SCHLICHTING, H. 1979. Boundary-layer theory, 7th ed. McGraw Hill.

SHAW, D. A., AND T. J. HANRATTY. 1977. Turbulent mass transfer rates to a wall for large Schmidt numbers. AIChE J. **23:** 28–37.

STEINBERGER, N., AND M. HONDZO. 1999. Diffusional mass transfer at the sediment–water interface. J. Environ. Eng. **125:** 192–200.

VAN DRIEST, E. R. 1956. On turbulent flow near a wall. J. Aeronautical Sci. **23:** 1007–1019.

Received: 30 November 2004
Accepted: 1 April 2005
Amended: 25 April 2005